https://doi.org/10.5194/egusphere-2025-6416
Preprint. Discussion started: 31 December 2025
© Author(s) 2025. CC BY 4.0 License.

Refining the Evolution of Gas-Particle Partitioning in Cooking Emissions Oxidation via FIGAERO-CIMS Analysis

Ruizhe Shen[1], Song Guo[1,2]*, Hui Wang[1#], Ying Yu[1#], Zichao Wan[1], Rui Tan[1], Wenfei Zhu[1], Zheng Chen[1], Shiyi Chen[1], Zhijun Wu[1], Shuangde Li[3], Yunfa Chen[3], Min Hu[1]

[1] *State Key Laboratory of Regional Environment and Sustainability, International Joint Laboratory for Regional Pollution Control, Ministry of Education (IJRC), College of Environmental Sciences and Engineering, Peking University, Beijing, 100871, China*

[2] *Collaborative Innovation Center of Atmospheric Environment and Equipment Technology, Nanjing University of Information Science & Technology, Nanjing 210044, China*

[3] *State Key Laboratory of Multiphase Complex Systems, Institute of Process Engineering, Chinese Academy of Sciences, Beijing 100190, China*

 # now at Institute of Climate and Energy Systems, Troposphere (ICE-3), Forschungszentrum Jülich, 52428, Germany

Corresponding author:

*Song Guo - State Key Laboratory of Regional Environment and Sustainability, International Joint Laboratory for Regional Pollution Control, Ministry of Education (IJRC), College of Environmental Sciences and Engineering, Peking University, Beijing, 100871, China; Email: songguo@pku.edu.cn

https://doi.org/10.5194/egusphere-2025-6416
Preprint. Discussion started: 31 December 2025
© Author(s) 2025. CC BY 4.0 License.

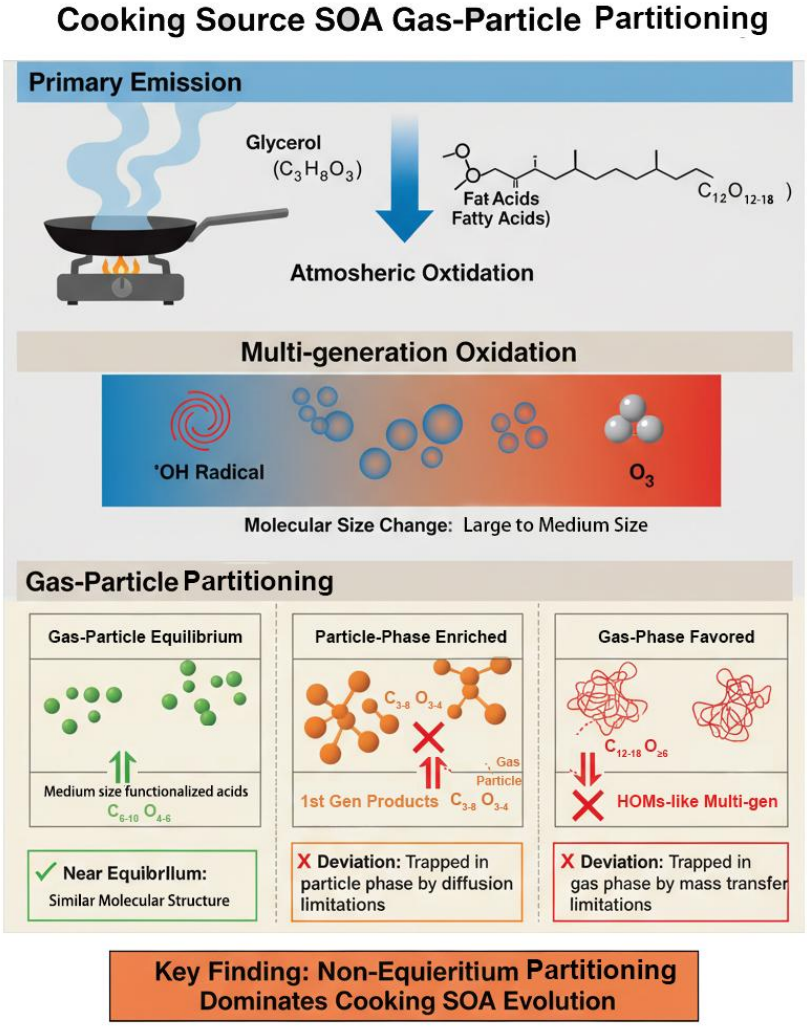

Graphical Abstract

https://doi.org/10.5194/egusphere-2025-6416
Preprint. Discussion started: 31 December 2025
© Author(s) 2025. CC BY 4.0 License.

ABSTRACT:

This study examines atmospheric oxidation and gas-particle partitioning of cooking-emitted organic aerosols. Using a Potential Aerosol Mass (PAM) flow reactor coupled with a Filter Inlet for Gases and AEROsols and a Chemical Ionization Mass Spectrometer (FIGAERO-CIMS), we monitored chemical composition, volatility distribution, and partitioning behavior under realistic conditions. A key aspect was applying high-resolution mass spectrometry within a two-dimensional volatility basis set (2-D VBS) framework to mechanistically analyze aerosol evolution. Experiments identified a two-stage particle formation: primary emissions rapidly produced fine particles (~10 nm) within two hours of oxidation, followed by secondary aerosol formation (30–50 nm) after 0.5–1 day of atmospheric aging. Oxidation products were primarily semi-volatile and intermediate-volatility organic compounds (S/IVOCs), shifting systematically toward semi-volatile organic compounds (SVOCs) over time, despite stable average molecular weight and oxidation state. Using Positive Matrix Factorization (PMF), we classified compounds by volatility and oxidation degree, identifying molecular markers for each stage. Highly oxidized small organic acids (⩽C3) and C7 – C10 multi-generation products were significant, showing moderate volatility and high oxidation states. A major finding was non-equilibrium gas-particle partitioning, strongly dependent on molecular class. Small organic acids and fragmentation products neared equilibrium, whereas first-generation oxidation products ($C_{3–8}O_{3–4}$) and large, non-fragmented compounds (>$C_{14}O_5$) exhibited kinetic limitations due to particle-phase diffusion constraints. This work enhances understanding of cooking aerosol behavior and provides a basis for improving emission inventories and air quality models.

Key Words: Secondary Organic Aerosol, Semi-volatile Organic Compounds, Intermediate-Volatility Organic Compounds, Gas-particle partitioning, FIGAERO CIMS, Cooking Emission

https://doi.org/10.5194/egusphere-2025-6416
Preprint. Discussion started: 31 December 2025
© Author(s) 2025. CC BY 4.0 License.

1. INTRODUCTION

Secondary organic aerosols (SOA) constitute a major component of submicron atmospheric particles on both global and regional scales. (Hallquist et al., 2009) Anthropogenic SOA, particularly prominent in densely populated regions, originate from and exert considerable impacts on human society(Guo et al., 2020). While emissions from industrial and transportation sectors have been increasingly regulated under clean-air initiatives, cooking emissions—associated with specific lifestyles—are emerging as significant sources of atmospheric volatile organic compounds (VOCs), semi-/intermediate-volatility organic compounds (S/IVOCs), and SOA precursors. Moreover, cooking represents a persistent source of indoor emissions in households, catering facilities, and restaurants, and accounting for over 20% of indoor activity time. Notably, indoor SOA formation may pose greater health risks than outdoor SOA in urban settings, given the substantial amount of time people spend indoors. Additionally, cooking emissions exhibit high spatial heterogeneity across urban areas, with emission profiles and environmental impacts varying considerably by regional culinary practices, leading to substantial uncertainties in emission estimates(Zhu et al., 2021). Therefore, effective clean-air policies aimed at mitigating cooking emissions require precise quantification of both emission characteristics and atmospheric transformation pathways.

Current research on cooking emissions has primarily focused on quantifying primary gaseous and aerosol components, along with variations linked to culinary practices. Key influencing factors encompass dish type (e.g., Eastern vs. Western cuisines, domestic cooking styles), ingredient profiles (food and oil varieties), and cooking conditions (oil temperature, seasoning usage, etc.). The gas phase is dominated by short-chain carbonyls and aliphatic acids, whereas the particle phase is rich in long-chain aliphatic acids. Other weakly oxygenated species derived from thermal decomposition and ingredient–oil interactions—such as sterols and polycyclic aromatic hydrocarbons (PAHs)—also contribute significantly to aerosol composition. (Lin et al., 2021) These emissions demonstrate strong SOA formation potential in urban, suburban, and even indoor environments. (Zeng et al., 2020;Guo et al., 2023) However, the gas-particle partitioning of organic compounds during the transformation of cooking emissions remains poorly understood, primarily due to the complexity and dynamic evolution of organic composition throughout emission and aging processes. This knowledge gap represents a major challenge in atmospheric chemistry. Since gas-particle partitioning directly influences the environmental and health impacts

https://doi.org/10.5194/egusphere-2025-6416
Preprint. Discussion started: 31 December 2025
© Author(s) 2025. CC BY 4.0 License.

of both primary and secondary organic aerosols, a mechanistic understanding of this process is essential for accurate risk assessment and effective air quality management.

In recent years, non-targeted analysis has advanced significantly for characterizing complex environmental mixtures in the absence of comprehensive calibration data. (Schymanski et al., 2015;Song et al., 2023a) This approach enables the extraction of diagnostic features from high-resolution mass spectrometry data to infer molecular characteristics and transformation pathways without prior structural knowledge. (Mazur et al., 2021) Widely applied in atmospheric science, non-targeted methods facilitate the identification of organic species from diverse sources and their environmental behaviors. (Song et al., 2023b;Pozza et al., 2023;Röhler et al., 2020;Hashimoto et al., 2022). While most techniques rely on chromatographic separation with high chemical resolution but limited temporal resolution. (Song et al., 2023b;Yang et al., 2023) This study integrates non-targeted analysis with high-resolution chemical ionization time-of-flight mass spectrometry (HR-ToF-CIMS) coupled to a Filter Inlet for Gases and Aerosols (FIGAERO). By employing matrix factorization and ordinal analysis, we aim to resolve the compositional features and gas–particle dynamics of cooking aerosols during oxidation, thereby elucidating the quantitative and compositional evolution of cooking-derived SOA under atmospheric conditions.

2. MATERIAL AND METHOD

2.1. Flow tube experiment setup. Flow tube oxidative evolution experiments of cooking emissions were conducted in a domestic lifestyle emission laboratory utilizing a Go:PAM Oxidation flow reactor (OFR) (Wang et al., 2021). The detailed information for the experiments were reported in the previous work (Yu et al., 2022). In brief, the Go:PAM reactor operates under mode OFR254 which generates OH from reaction between $O(^1D)$ radical, formed by photo-oxidation of ozone under ultraviolet dissociation at 254 nm, and water vapor, representing oxidation process dominated by OH radical and ozone at low NO_x concentration(Peng and Jimenez, 2020). Thus, during the experiment, OH exposure in the Go:PAM system was controlled by varying ozone concentration from the ozone generator, relative humidity from the humidifier, and the experimental sample gas flow rate through the Go:PAM reactor. OH exposure is estimated using empirical equations in OFR recommended by Peng et al(Peng et al., 2016). Cooking experiments were conducted in a custom-made fry pan directly connect to pure nitrogen as carrier gas to avoid interference of high NO_x in ambient air on radical oxidation. Emissions were generated by heating corn oil to 120~130 °C, representing the evolution of widely used cooking

https://doi.org/10.5194/egusphere-2025-6416
Preprint. Discussion started: 31 December 2025
© Author(s) 2025. CC BY 4.0 License.

oil during typical domestic cooking activities in both Eastern and Western cooking types(Abdullahi et al., 2013;Bandowe et al., 2021). Detailed experimental conditions are presented in section S1 in Supplement Information 1.

2.2. Instrumentation setup. For oxidative conditions in the Go:PAM reactor, ozone concentration are monitored using Thermo® model 49i ozone analyzer. Organic species in the gas phase, including precursors and low-molecular-weight oxidation products, are quantified on-line using VOCUS-PTR instruments. Particle size distribution before and after Go:PAM oxidation are measured by two Scanning Mobility Particle Sizer (SMPS) systems, before one consist of TSI® model 3080 DMA & model 3776 CPC and after one model 3082 DMA & model 3772 CPC. Particle density measurement adopted Cambustion® Centrifugal Particle Mass Analyzer (CPMA) for total mass estimation at various oxidation state. Molecular composition, gas-particle partitioning, and volatility of organic aerosols and are determined by a FIGAERO inlet coupled to HR-ToF-CIMS instrumentation developed by Aerodyne Inc® that choose iodide as reagent ion. Operation of FIGAERO-CIMS instrument in laboratory oxidation experiments has been since the instrumentation firstly developed (Lopez-Hilfiker et al., 2014;Le Breton et al., 2019;Bannan et al., 2019). Briefly, the FIGAERO inlet consists of a gas-phase inlet that pull air directly into the API interface and IMR of CIMS instrument, and an aerosol inlet that collect aerosol sample on a PTFE filter. One analyzes cycle is completed by a 15-min gas-phase inlet sampling period while particles collected onto the filter at aerosol inlet, a 15-min particle phase thermal desorption period when the temperature on the filter increase linearly from home temperature to 180°C, a 15-min continuous heating scheme and a 15-min cooling scheme. FIGAERO offers the ability of determining both gas phase and particle phase concentration and thus gas-particle partitioning information from CIMS data measurement in different period (Lopez-Hilfiker et al., 2016). For example, gas-particle partitioning coefficient K_p, defined similar to phase- equilibrium coefficients between gas-phase and particle-phase organic species, can be determined by average CIMS signal during gas-phase, during aerosol phase, and OA concentration measured by mass concentration instruments such as SMPS or AMS. Moreover, volatility of organic species can be determined by thermal desorption characteristics during linear heating process in the measurement cycle(Bannan et al., 2019). Both concentration and volatility quantification require certain calibration processes and authentication standard(Ylisirniö et al., 2021). Detailed operation and data process of various instruments, sensitivity & volatility calibration methods, and quantification of species without

https://doi.org/10.5194/egusphere-2025-6416
Preprint. Discussion started: 31 December 2025
© Author(s) 2025. CC BY 4.0 License.

authentication standard are presented in Section S2 in Supplement 1. Detailed gas-particle partitioning and volatility assignment methods from FIGAERO-CIMS data are shown in Section S5 in Supplement 1.

2.3. Two-Dimensional Volatility Basis Set (2-D VBS) framwork for composition representation. The Two-Dimensional Volatility Basis Set (2-D VBS) framework has been developed to characterize the complex composition of organic aerosols in laboratory experiments, ambient observations, and modeling studies. This approach distributes organic species in 2-D gridded area with variation of mean carbon oxidation state $\overline{OS_c}$ and saturation vapor concentration C^*(Donahue et al., 2011;Donahue et al., 2012;Chuang and Donahue, 2016). The result gas- and particle-phase composition and partitioning coefficients of primary emissions and secondary oxidation experiments are shown in 2-D VBS space to intuitively show the evolution of organic aerosol and its partitioning characteristics. Saturation vapor concentration in the 2-D VBS space are estimated using elemental composition from CIMS detection using an empirical parameterization recommended by Li et al.(Li et al., 2016), shown in the section S3 in Supplement Information 1.

2.4. Non-targeted analysis of FIGAERO-CIMS data by Matrix Factorization. HR-ToF-CIMS enables the detection of thousands of ions, corresponding to a comparable number of chemical species. In the present study, the FIGAERO-CIMS instrument detected more than 800 assignable ions that can be matched to specific compounds in both gas phase and secondary organic aerosol (SOA). To extract meaningful compositional and volatility patterns from the complex dataset of experimental concentration profiles, we applied Positive Matrix Factorization (PMF) via the Igor Pro®-based SoFi® software. Additionally, ordinal analysis methods, as previously established and applied by Kong et al. in factor interpretation, were adopted to identify the most abundant compounds within each resolved factor. (Kong et al., 2021).

3. RESULT AND DISCUSSION

3.1. Evolution of Size and Mass Distributions of Cooking Organic Aerosols under Oxidation.

The evolution of size and mass distributions for primary and secondary organic aerosols throughout oxidation are presented in Figure 1 and Table 1. Primary cooking aerosols exhibit a relatively broad size distribution, with particle diameters ranging from 50 to 300 nm. These particles are generally formed through physical processes such as oil evaporation or thermal

https://doi.org/10.5194/egusphere-2025-6416
Preprint. Discussion started: 31 December 2025
© Author(s) 2025. CC BY 4.0 License.

chemical reactions including oxidation and decomposition. As a result, they comprise components with large molecular size and relatively low carbon oxidation states, such as long-chain alkanes, alkenes, alkanals, alkenones, fatty acids and their glycerol esters, and steroids.(Rogge et al., 1991;Nolte et al., 1999).

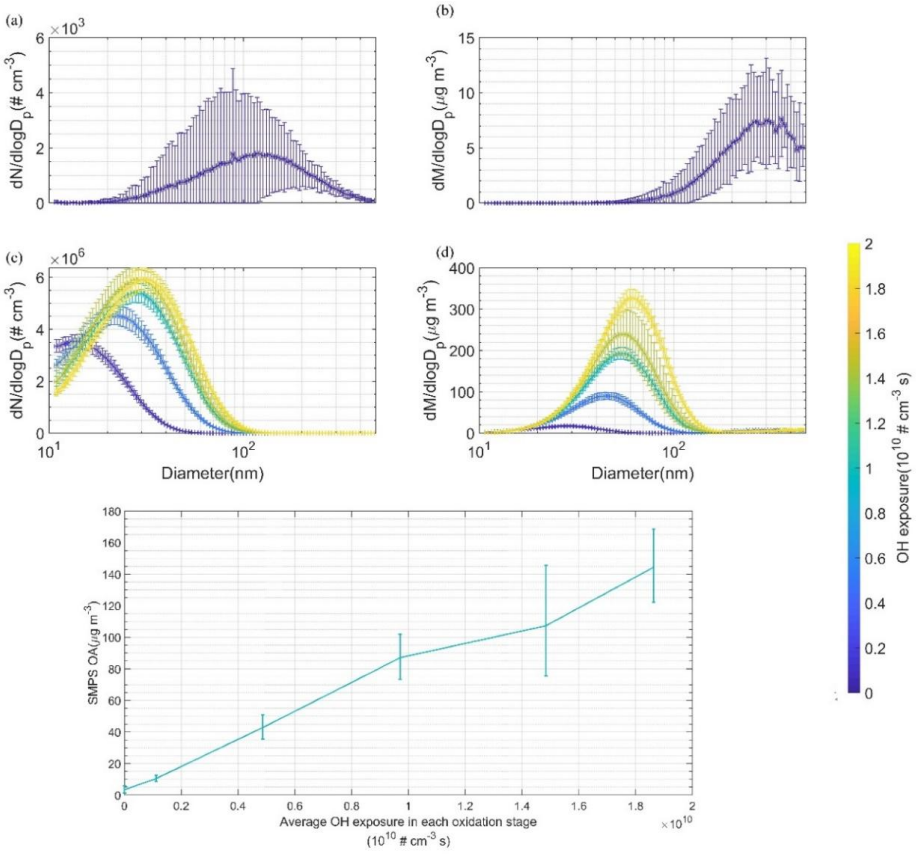

Figure 1 Primary and Secondary aerosol size & mass distribution evolution with oxidation age increases. (a) stands for number distribution, (b) mass distribution of primary particles, (c) (d)number distribution & mass distribution of secondary aerosols in Go:PAM flow tube at OH radical exposure 0.1~1.8×10^{10} cm^{-3} s (e) mass concentration evolution with oxidation process from primary to ~1.8×10^{10} cm^{-3} s

In contrast, secondary organic aerosols are predominantly nanoparticles with diameters below 50 nm, exhibiting a substantial increase in both number and mass upon oxidant exposure. Even under the lowest OH concentration conditions, secondary aerosol number concentrations can

https://doi.org/10.5194/egusphere-2025-6416
Preprint. Discussion started: 31 December 2025
© Author(s) 2025. CC BY 4.0 License.

reach up to 10^6 #·cm^{-3}. Increasing OH exposure further enhances mass concentration primarily through particle size growth rather than number increase. This observation implies that the gas-particle partitioning of secondary organic species does not reach equilibrium. Notably, particles larger than 90 nm show minimal changes in number or mass concentration, with average declines of less than 20% even under the strongest oxidation conditions (Figure S19). These findings collectively suggest that secondary organic aerosols from oil boiling originate mainly from nucleation and condensation of gas-phase oxidation products, rather than from oxidative aging of primary aerosols.** The observed low reactivity of primary cooking aerosols during oxidation may be attributed to the low miscibility between nonpolar or low-polarity primary components and highly polar secondary compounds (Chandramouli et al., 2003;Milsom et al., 2021) , likely resulting from limited partitioning tendency of primary components.

Table 1 Mean 2-D VBS parameters of primary and secondary cooking organic aerosols

OH radical exposure (10^{10} cm^{-3}·s)	Mean molecular composition	$\log_{10}C^*$(μg·m^{-3})	Mean OS_C
Primary	$C_{3.5}H_{5.4}O_{2.6}N_{0.03}S_{0.01}$*	6.0*	-0.11*
	$C_{7.1}H_{10.3}O_{3.8}N_{0.09}S_{0.03}$**	2.8**	-0.47**
0.488	$C_{5.8}H_{9.5}O_{3.7}N_{0.07}S_{0.04}$*	3.5*	-0.45*
	$C_{7.3}H_{11.9}O_{3.8}N_{0.04}S_{0.01}$**	2.8**	-0.63**
0.971	$C_{6.6}H_{10.6}O_{4.0}N_{0.07}S_{0.05}$*	2.8*	-0.49*
	$C_{7.8}H_{12.9}O_{4.0}N_{0.04}S_{0.01}$**	2.4**	-0.67**
1.86	$C_{7.0}H_{11.0}O_{4.2}N_{0.07}S_{0.06}$*	2.3*	-0.47*
	$C_{7.8}H_{13.0}O_{4.1}N_{0.04}S_{0.01}$**	2.2**	-0.65**

* Gas phase

**Aerosol phase

3.2 Composition and volatility distribution of primary and secondary organic aerosols in 2-D VBS Space. Figure 2 displays the volatility and compositional distribution of cooking aerosols and associated gas-phase organic components within the two-dimensional volatility basis set (2-D

https://doi.org/10.5194/egusphere-2025-6416
Preprint. Discussion started: 31 December 2025
© Author(s) 2025. CC BY 4.0 License.

VBS) framework (Donahue et al., 2012). The majority of primary and secondary organic species are distributed in the semi-volatile and intermediate-volatile organic compound (S/IVOC) range, with an average carbon oxidation state (OSc) spanning from –1.25 to 0.5. Throughout the oxidation experiment, increasing OH exposure led to a substantial growth in S/IVOC components, consistent with the trend observed for aerosol particles. Additionally, the formation of low-volatility, highly oxidized compounds derived from multi-generation oxidation is also promoted.

In the gas phase, the average molecular size increases significantly during oxidation, whereas the carbon oxidation state remains nearly constant or exhibits a slight decrease following OH radical addition. This behavior may be attributed to the generation of gas-phase oxidation products via cleavage of primary long-chain fatty acids, polymerization among oxidation intermediates, and the depletion of primary low-molecular-weight organic acids resulting from glycerol thermal decomposition, such as formic acid, acetic acid, and glyceric acid (Zhang et al., 2018;Takhar et al., 2022). By contrast, compositional shifts in the aerosol phase within the 2-D VBS space—such as in oxidation state and molecular size—are relatively minor compared to those in the gas phase. The oxidation state of particle-phase organics remains largely unchanged, with only marginal growth in molecular dimensions.** The relatively small molecular size of primary cooking aerosols may result from the limited detection sensitivity of iodide-adduct CIMS toward nonpolar or low-polarity compounds with large molecular weights and fewer oxygen-containing functional groups, e.g., long-chain hydrocarbons, fatty acids, and steroids (Iyer et al., 2016). These compositional patterns suggest that aerosol growth is governed primarily by the condensation of secondary S/IVOCs from the gas phase, rather than by continued oxidation within the particle phase. This observation implies that the oxidation process in the flow tube has approached a "steady-state turning point," particularly for particle-phase products, which reach this stage earlier owing to their oxygen-rich nature, such as dicarboxylic acids and hydroxy acids with carbon numbers greater than six. These products, formed through oxidation of long-chain primary acids and carbonyls, exhibit lower volatility and higher viscosity, thereby slowing subsequent oxidative aging (Milsom et al., 2021). Detailed 2-D VBS distribution of primary and secondary organic matter in gas and aerosol phase are shown in **Supplementary Material S2**.

https://doi.org/10.5194/egusphere-2025-6416
Preprint. Discussion started: 31 December 2025
© Author(s) 2025. CC BY 4.0 License.

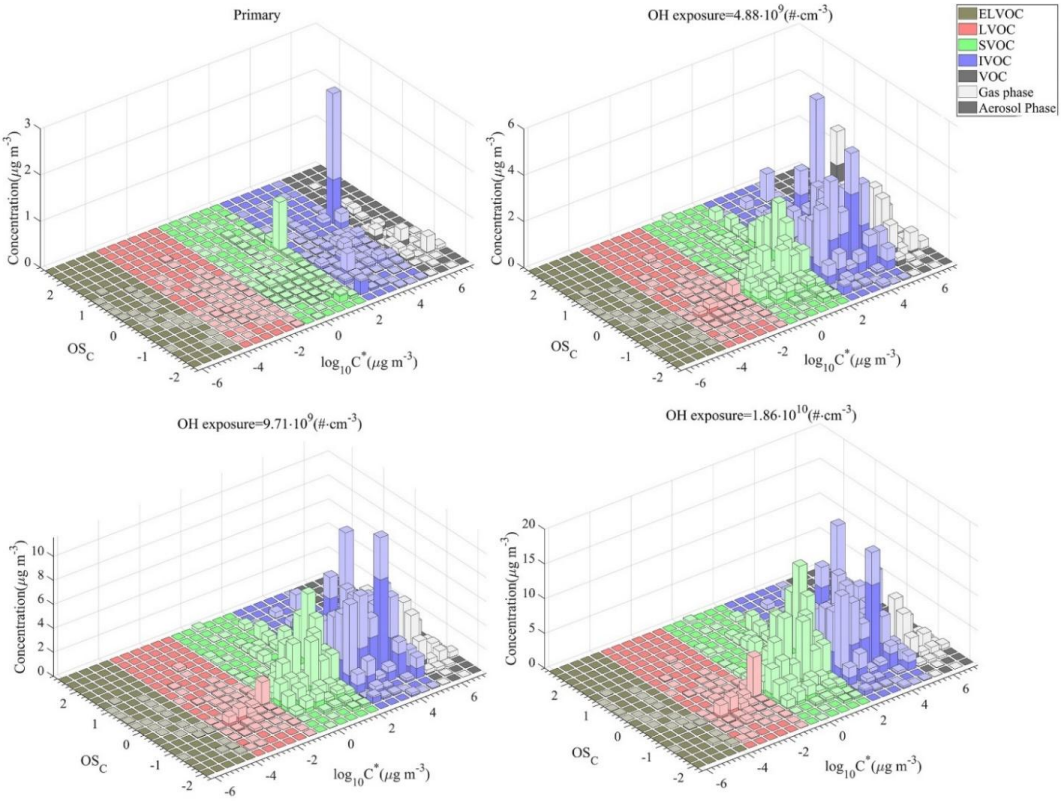

Figure 2 Composition distribution of gas-phase and aerosol-phase cooking organic species in 2-D VBS space

3.3 Classification and Quantification of Primary and Secondary Cooking Emissions by Non-targeted Analysis. ME-2 PMF methods are adopted in deconvolution and non-targeted analysis of FIGAERO-CIMS detections on gas-phase and aerosol-phase organic compounds with different volatility and oxidative state, so as to classify typical organic species, and then extract evolution pattern corresponding to oxidation mechanism and changes of gas-particle partitioning from complex CIMS data matrix(Buchholz et al., 2020;Hashimoto et al., 2022;Kong et al., 2021). Detailed PMF recommended factor determination methods are shown in Section S4 of Supplement S1. Figure 3 shows the recommended NTA results of FIGAERO-CIMS data. The FIGAERO-CIMS results are divided to 13 factors, 5 pure gas-phase factors, 3 semi-volatile factors with considerable and comparable amount both in gas phase and aerosol phase, and 5 aerosol-phase factors. Factors are listed in **Figure 3** and classified by its volatility (partitioning coefficient K_p

https://doi.org/10.5194/egusphere-2025-6416
Preprint. Discussion started: 31 December 2025
© Author(s) 2025. CC BY 4.0 License.

while total amount is countable) and oxidative state (mean oxidative state OS_C and evolution with enhancement of oxidation). Detailed classification procedure are shown in Section S4 of the Supplement S1. Formic acid (at m/z 173, detected as $ICH_2O_2^-$ in CIMS) are not included in PMF analysis due to its extreme high abundant in gas phase of primary emissions and low oxidative states compared to other species (up to 25ppb), as shown in Figure S21. High abundant of formic acid at ppb in indoor sources and cooking emissions at ppb level has been reported before(Reyes-Villegas et al., 2018;Farmer et al., 2019). Formation of cooking originated formic acid possibly due to thermal decomposition of glycerol in primary species (Takhar et al., 2022;Nolte et al., 1999;Farmer et al., 2019). Primary formic acid would decline slower than estimated from OH radical reactivity (formic acid decline about 22% at OH exposure 10^{10} $cm^3 \cdot s^{-1}$) at current oxidative stage(Farmer et al., 2019;Atkinson et al., 2006), showing existence of other possible consumption pathways such as photolysis. Decline of formic acids with OH radical enhancement is slower than estimation from formic acid OH reactivity, indicating that secondary formic acids are also formed, possibly by ozonolysis and further oxidation of unsaturated long-chain organic acids(Farmer et al., 2019;Takhar et al., 2021).

Among factors, we would first classify the 13th factor as more closely to contaminant factor as shown in **Figure S22**, because of its unreasonable temperature distribution at thermal desorption state. We would call this factor "Unknown", apart from other factors that are classified from their volatility and oxidative states. Total concentration of contaminant factor Unknown is relatively low, showing that contaminant would not be able to interfere measurement result too much. In ordinary factors from Factor V1 to Factor LV4, Factor V1 and Factor SV1 are first classified relate to primary emissions. The average elemental composition and most abundant species of Factor V1 and Factor SV1 are shown in **Table S7-S8**. **Factor V1** stands for gas-phase primary emission, mainly consist of low-molecular-weight oxygenated organic compounds such as short chain carboxylic acids and their deviates(Masoud et al., 2022). Most abundant compounds in Factor V1 are $C_{1\text{-}3}$ oxygenated organic species, such as $C_2H_4O_2I^-$ (m/z 186.92, iodide adduct) corresponding to acetic acid, $C_3H_4O_2I^-$ (m/z 198.93, iodide adduct) corresponding to acrylic acid, $C_3H_8O_3I^-$ (m/z 218.95, iodide adduct) corresponding to glycerol. These compounds probably originate from thermal oxidation or thermal decomposition of glycerol, which are formed by thermal decomposition of oil esters(Nolte et al., 1999;Lopez-Pedrajas et al., 2018;Reyes-Villegas et al., 2018). Next abundant compounds in **V1** are larger less-oxygenated compounds with carbon

https://doi.org/10.5194/egusphere-2025-6416
Preprint. Discussion started: 31 December 2025
© Author(s) 2025. CC BY 4.0 License.

number >5 and oxygen number ≤2, probably formed from thermal decomposition of fat followed by thermal oxidation processes long-chain aliphatic acids(Takhar et al., 2022;Takhar et al., 2021;Nolte et al., 1999). The examples are $C_6H_{12}O_2I^-$ (m/z 242.99, iodide adduct) corresponding to hexanoic acid and $C_5H_{10}O_2I^-$ (m/z 228.97, iodide adduct) corresponding to pentatonic acid. Semi-volatile factor **SV1** contains semi- and intermediate- volatile organic compounds with medium carbon number (5 carbons on average) and higher oxidative state than V1. Most abundant compounds are $C_{3\text{-}6}$ and $O_{2\text{-}3}$ compounds, which may correspond to organic acid derivatives, such as hydroxy acids and carbonyl acids that originate from thermal oxidation of long-chain aliphatic acid in primary emissions. Compound detected as $C_5H_4O_4I^-$ (m/z 254.91, iodide adduct), possibly corresponding to aconic acid or hydroxy furoic acid, has the highest intensity in **SV1**. $C_5H_4O_4$ present mostly in gas phase during primary emission, while particle-phase abundance increases with oxidation age increasing, indicating its possible primary thermal oxidation and dehydration origin, leading to gas-phase degradation and partitioning toward aerosol phase. Other compounds abundant in **SV1** with similar evolution characteristics includes long-chain aliphatic acids, such as palmitic acid ($C_{16}H_{32}O_2I^-$, m/z 383.14, iodide adduct), oleic acid ($C_{18}H_{34}O_2I^-$, m/z 409.16, iodide adduct), stearic acid ($C_{18}H_{36}O_2I^-$, m/z 411.17, iodide adduct), and glycerol ($C_{18}H_{34}O_2I^-$, m/z 409.16, iodide adduct). These typical primary organic compounds have evolution trends similar to $C_5H_4O_4$, with increasing are apparently abundant in gas phase and aerosol phase, but with lower concentration than small molecules ones, probably due to the quantification uncertainty of sensitivity estimation of lower-oxygenated long-chain organics(Lee et al., 2014). Other Gas-particle partitioning of typical species divided into **SV1** such as $C_5H_8O_3I^-$ (m/z 254.91, iodide adduct) and $C_5H_8O_3I^-$ (m/z 254.91, iodide adduct) show different evolution pattern other than primary compounds, implementing possible two distinct origins of these compounds: primary formation from gas-phase thermal oxidation, and secondary formation from OH radical oxidation or ozonolysis of primary emissions.

Factors with intermediate oxidative state are **V2**, **V3**, **SV2** and **LV1** that achieve highest abundance at medium oxidative stage. Among these factors, factor **V2** and **LV1** are factors with smaller molecules, reach its peak concentration at lower oxidative stage， while**V3** and **SV2** exhibits maximum at higher oxidative state and contains more larger molecules. More typical intermediate oxidative state volatile factor **V2** mainly consist of two distinct categories of species. One is $C_{2\text{-}3}$ oxygenated compounds that are higher-oxidized than in factor **V1**, such as $C_3H_4O_3I^-$

https://doi.org/10.5194/egusphere-2025-6416
Preprint. Discussion started: 31 December 2025
© Author(s) 2025. CC BY 4.0 License.

(m/z 214.92, iodide adduct, possibly pyruvic acid) and $C_2H_4O_4I^-$ (m/z 214.92, iodide adduct) that may originate from first-generation radical oxidation or ozonolysis of glycerol-related compounds. The other is $C_{4\text{-}7}$ oxygenated compounds at intermediate oxidative stage with medium oxidative state, such as $C_5H_{10}O_3I^-$ (m/z 244.97, iodide adduct) and $C_7H_{12}O_3I^-$ (m/z 214.92, iodide adduct), corresponding to first-generation scissoring product of long-chain fatty acids during radical oxidation or ozonolysis, or first-generation oxidation of thermal decomposition products(Liu et al., 2024;Takhar et al., 2022;Takhar et al., 2021). Factor **LV1** have similar average oxidative state and molecular size with Factor **V2**, seems corresponding to gas phase portion of first-generation oxidation products represented by Factor **V2.** However, thermal desorption thermogram of Factor **LV1** peaks at ~440K, showing that compounds represented by Factor **LV1** have much lower volatility than molecular composition corresponding to this factor, showing Factor **LV1** would be exactly thermal decomposition products of large molecules generated from oxygen-addition of long-chain fatty acids without scissoring reaction(Brown et al., 2021;Lopez-Hilfiker et al., 2019), which may have elemental composition of $C_{16/18}H_{30\text{-}34}O_{3\text{-}6}$. Particle-phase reactions between possible peroxides (such as $C_7H_{12}O_5$ and $C_9H_{16}O_5$ that abundant in Factor **V2** and **LV1**) and substituted alcohols or aldehydes ($C_6H_{12}O_3$ or $C_6H_{10}O_3$, etc.) accelerated by thermal desorption at lower oxidative stage may also be an alternative source(Luo et al., 2024). Volatile factor **V3** and semi-volatile Factor **SV2** share similar molecular composition such as overall oxidation state, molecular size and typical species. These species, mostly $C_{4\text{-}6}$ acids in gas phase and $C_{9\text{-}10}$ carbonyl acids in aerosol phase, have larger molecular size. These factors are totally generated from oxidation of fatty acids rather than compounds related to glycerol that are abundant in lower-oxidative-stage factors. Moreover, comparing thermal desorption properties with molecular composition, species in Factor **SV2** represent compounds with exact molecular formula detected by CIMS rather than thermal decomposition products. Overall, Typical intermediate compounds are pyruvic acid in gas phase, $C_{5\text{-}10}$ carbonyl acids in both phase and large-molecular oxidation products $C_{16/18}H_{30\text{-}34}O_{3\text{-}4}$ in the aerosol phase.

Highly-oxygenated factors are Factor **V4**, Factor **V5**, Factor **SV3** and Factor **LV2-LV4** that reach highest intensity at highest experimental oxidative stage. Among factors, Factor **V4** and **LV2** are lesser oxidized, the amount of these factors reaches steady state while oxidative stage increases to maximum in the experiment. Other factors are highly oxidized: their abundance increases significantly during oxidative stage growth. Typical gas phase species are highly oxidized

https://doi.org/10.5194/egusphere-2025-6416
Preprint. Discussion started: 31 December 2025
© Author(s) 2025. CC BY 4.0 License.

termination products of glycerol-related species, such as $C_3H_4O_4I^-$ (m/z 230.91, iodide adduct, probably malonic acid) and $C_3H_6O_4I^-$ (m/z 232.93, iodide adduct, probably glyceric acid), or low-molecular-weight fragmentation products of fatty acid oxidation, such as $C_4H_6O_4I^-$ (m/z 244.93, iodide adduct, probably succinic acid). These highly oxidized low-molecular weight compounds are more semi-volatile rather than volatile species. Aerosol phase compounds are mostly $C_{7\text{-}10}H_{12\text{-}16}O_{4\text{-}6}$ compounds that may corresponding to $C_{7\text{-}10}$ organic acids, diacids, and its derivates. Typical species include $C_9H_{16}O_4I^-$ (m/z 315.01, iodide adduct, probably azelaic acid), $C_9H_{18}O_4I^-$ (m/z 317.03, iodide adduct, possibly dihydroxy or hydroperoxyl C_9 carboxylic acid), and $C_{10}H_{18}O_4I^-$ (m/z 329.03, iodide adduct, possibly oxo- hydroxy C_{10} carboxylic acid). Highly oxygenated species with 6 oxygen atoms and more are abundant in those low-volatile factors compared to intermediate-oxidative state factors. These larger molecule oxidation products have similar oxidative state and lower saturation vapor pressure, thus are more abundant in the aerosol phase.

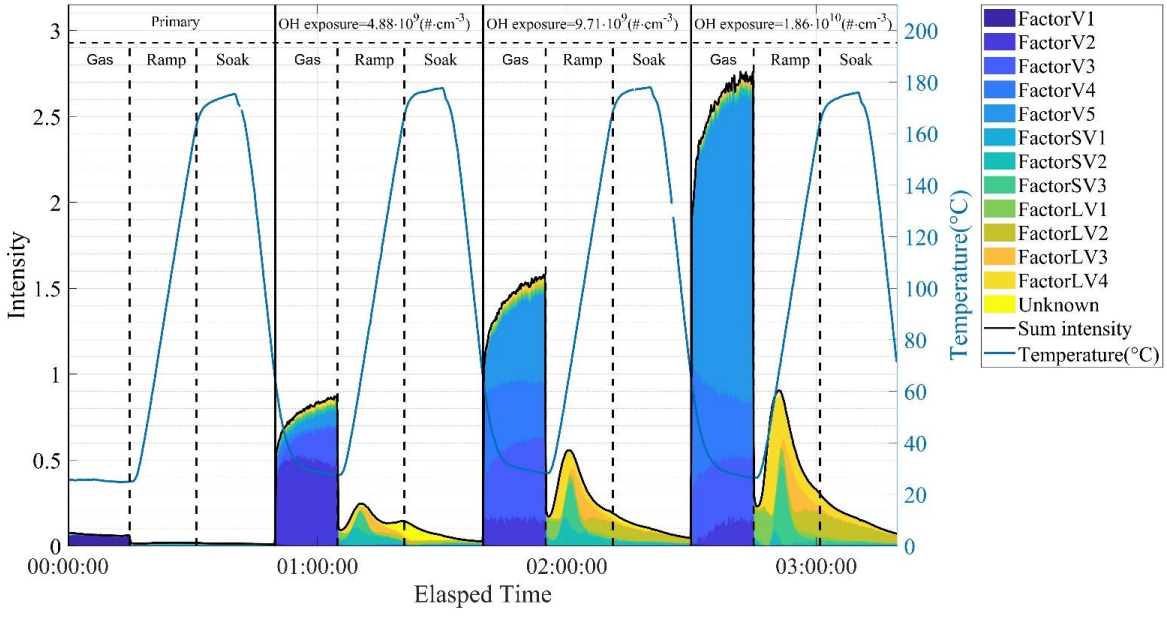

Figure 3 non-targeted classification result time series with evolution of experiment state. Y-axis Intensity represents the sum of CIMS organic signal normalized to iodide ion other than formic acid.

3.4 Gas-particle partitioning of typical species. Typical species and its evolution in each oxidative stages during formation and aging of cooking emissions are listed in composition tables

https://doi.org/10.5194/egusphere-2025-6416
Preprint. Discussion started: 31 December 2025
© Author(s) 2025. CC BY 4.0 License.

in Section S6 of SI. Among those species, highly-volatile low-molecular-weight compounds, such as formic acid and acetic acid, are typically gaseous species. The abundance of these volatile species detected in "aerosol phase" are probably resulting from thermal decomposition. We would then mainly focus on semi-volatile and low-volatile species with considerable gas-particle partitioning influence on SOA formation and evolution. These key species, including primary species related to cooking emissions(Reyes-Villegas et al., 2018), intermediate oxidative state species related to first-generation oxidation or thermal oxidation(Takhar et al., 2022), and multi-generation termination oxidation products(Masoud et al., 2022;Brown et al., 2021;Takhar et al., 2021), are listed in **Table 3**.

Table 3 Classified typical species at various oxidative stage

Oxidative stage	Volatility	Formula	Possible species	p^0(Pa,25°C)
Primary	Semi-volatile	$C_3H_8O_3$	Glycerol	2.24×10^{-2}
		$C_{16}H_{32}O_2$	Palmitic acid	2.67×10^{-5}
		$C_{18}H_{34}O_2$	Oleic acid	1.12×10^{-4}
First-generation	Semi-volatile	$C_3H_4O_3$	Pyruvic acid	1.72×10^{2}
		$C_7H_{12}O_3$	-	1.18×10^{0}
		$C_{10}H_{16}O_3$	-	1.09×10^{-1}
	Low-volatile	$C_{16}H_{32}O_3$	-	6.96×10^{-6}
Multi-generations	Semi-volatile	$C_4H_6O_4$	Succinic acid	1.04×10^{-3}
		$C_6H_{10}O_4$	Adipic acid	5.4×10^{-4}
		$C_9H_{16}O_4$	Azelaic acid	4.74×10^{-5}
	Low-volatile	$C_{10}H_{18}O_5$	-	4.02×10^{-5}
		$C_{18}H_{32}O_6$	-	1.39×10^{-8}

https://doi.org/10.5194/egusphere-2025-6416
Preprint. Discussion started: 31 December 2025
© Author(s) 2025. CC BY 4.0 License.

Figure 4 summarized the gas-particle partitioning of typical species chosen in **Table 3**, representing gas-particle partitioning characteristics of species with varying oxidative stage, illustrating the discrepancies between estimated and experimental values of the partitioning coefficient (K_p) for typical components at varying oxidation degrees as the oxidation process progresses. The subplot legends indicate the oxidation degree of each component, where dashed lines represent estimated values and solid lines denote experimental values. Specifically, among primary emission components, the gas-particle partitioning of fatty acid-like large molecule components is consistent with ideal gas-liquid equilibrium scenario with an activity coefficient ξ close to unity, whereas glycerol-related components exhibit a more pronounced deviation. With oxidation proceeds leading to SOA formation, the partitioning coefficient of primary components decreases significantly, indicating that changes in the particle-phase composition influence the activity coefficient and partitioning kinetics of primary components. Among first-generation oxidation products, components with C_5 and higher carbon numbers predominate, primarily originating from fatty acid cleavage, while a minority of C_4 and lower components derive from glycerol oxidation. The theoretical K_p values for C_5 and higher first-generation oxidation products generated via scissoring reactions are markedly lower than the estimated values, indicating a substantial deviation from equilibrium in their gas-particle partitioning. Multi-generation oxidation products exhibit less deviation with estimated due to its similarity with aerosol bulk composition; However, large molecule oxidation products (e.g., $C_{18}H_{32}O_6$) demonstrate significant deviations. Estimates based on equilibrium partitioning suggest that these components should only occupy a minimal fraction in the gas phase; however, measurement results in substantial gas-phase presence.

https://doi.org/10.5194/egusphere-2025-6416
Preprint. Discussion started: 31 December 2025
© Author(s) 2025. CC BY 4.0 License.

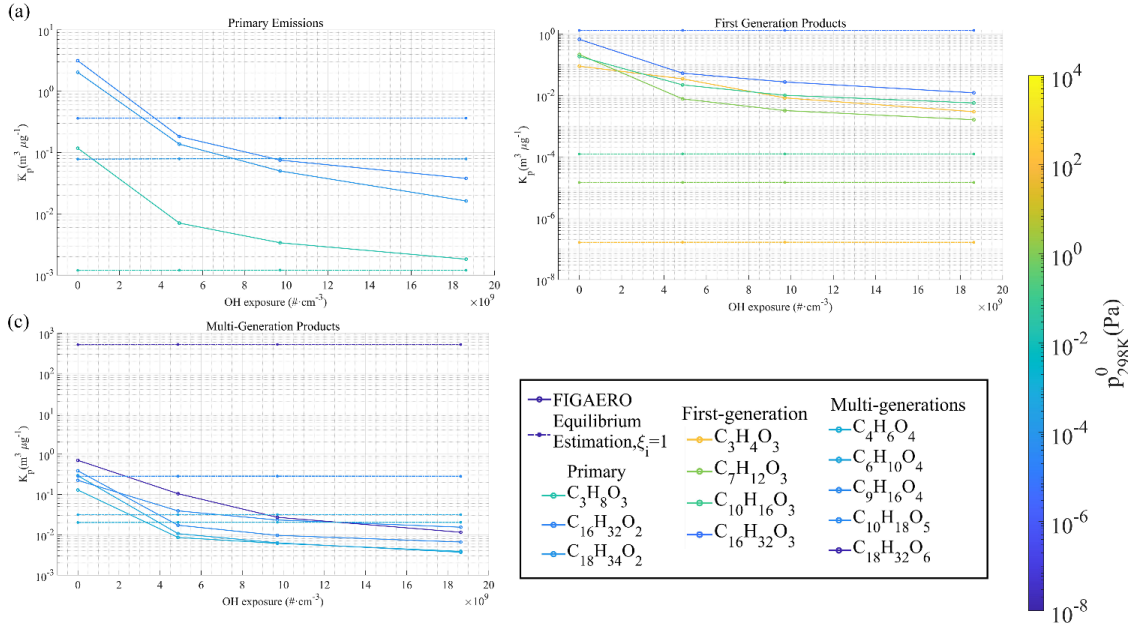

Figure 4 measurement and estimated partitioning coefficient (K_p) evolution of typical species of (a) primary emission (b) first generation products (c) multi-generation oxidation products

Overall, due to diffusion limitations, the gas-particle partitioning of medium molecular weight–medium oxidation state ($C_{3-8}O_{3-4}$) primary components and first-generation oxidation products, as well as large molecule with high oxidation state ($C_{\geq 12}O_{\geq 6}$) products deviates significantly from ideal-state estimates. The theoretical estimate approach overestimates the partitioning coefficient of $C_{3-8}O_{3-4}$ compounds and underestimates that of $C_{\geq 12}O_{\geq 6}$ compounds. The deviation in component gas-particle partitioning from the ideal state may arise from two factors: First, the activity coefficient ξ of species influences gas-particle partitioning. The theoretical K_p values shown in the figure assume the particle phase to be an ideal organic solution, with the activity coefficient ξ consistently equal to 1; in reality, however, changes in particle-phase composition cause the activity coefficient ξ to deviate from ideal conditions, thereby affecting partitioning behavior. Second, gas-particle partitioning may deviate from gas- 'liquid' equilibrium. If their exists kinetic limitations of composition mass transfer, estimations based on theoretical equilibrium gas-phase dissolution become invalid. During the rapid particle formation stage at lower oxidative state, medium molecular weight–medium oxidation state($C_{3-8}O_{3-4}$) components rapidly condense to form fine aerosols as most particle-phase contributors. With particle size

https://doi.org/10.5194/egusphere-2025-6416
Preprint. Discussion started: 31 December 2025
© Author(s) 2025. CC BY 4.0 License.

further increases, kinetic limitations in gas-particle partitioning hinder their re-evaporation and gas-phase oxidation, trapping them in the particle phase(Shiraiwa et al., 2012;Zhang et al., 2012;Zaveri et al., 2018). In contrast, for high-oxidative-state large molecules, diffusion and surface mass transfer limitations impede their entry into the particle phase, resulting in their persistence in the gas phase(Zaveri et al., 2018;Masoud et al., 2022;Schervish and Shiraiwa, 2023). Measurement uncertainties related to thermal desorption as an intrinsic property of FIGAERO-CIMS may also contribute to the observed deviations(Mehra et al., 2020;Tikkanen et al., 2020;Masoud et al., 2022).

4. CONCLUSIONS

Our study presents a comprehensive investigation into the atmospheric evolution of cooking-derived organic aerosols, integrating advanced analytical techniques to unravel complex gas-particle dynamics. By employing a PAM flow tube oxidation system coupled with FIGAERO-CIMS technology, we quantitatively tracked changes in chemical composition, volatility, and gas-particle partitioning throughout oxidation. A key innovation lies in the combined application of high-resolution mass spectrometry with a two-dimensional volatility basis set (2-D VBS) framework, enabling a mechanistic understanding of composition-dependent partitioning behavior.

Under typical atmospheric conditions, primary cooking emissions rapidly generated substantial quantities of fine particles (~10 nm) within two hours, followed by the formation of higher concentrations of 30–50 nm secondary aerosols over 0.5-1 days. Notably, oxidation products predominantly occupied the semi-volatile and intermediate-volatility organic compounds (S/IVOCs) range in the 2-D VBS, systematically migrating toward the SVOC region as oxidation progressed, while molecular weight and oxidation degree remained relatively stable. Leveraging positive matrix factorization (PMF), we systematically classified compounds by oxidation degree and volatility, identifying representative markers across evolution stages: gaseous glycerol and particulate long-chain fatty acids in primary emissions; medium-weight carbonyl acids (e.g., $C_5H_{10}O_3$, $C_7H_{12}O_3$) as intermediate products, and multi-generation oxidation products including dicarboxylic acids (e.g., $C_9H_{16}O_4$) and HOM-like compounds (e.g., $C_{18}H_{32}O_{5–6}$) as mature products. Of particular importance are highly oxidized small organic acids (⩽C3) and multi-generation products in the C7-C10 range with moderate volatility and high oxidation state.

A central finding concerns the non-equilibrium gas-particle partitioning observed across different compound classes. While small organic acids and scission-derived multi-generation

https://doi.org/10.5194/egusphere-2025-6416
Preprint. Discussion started: 31 December 2025
© Author(s) 2025. CC BY 4.0 License.

products approached theoretical equilibrium, we identified significant kinetic limitations for first-generation oxidation products ($C_{3–8}O_{3–4}$) and large non-cleavage products ($>C_{14}O_5$), which exhibited significant deviations due to particle-phase diffusion and mass transfer constraints. This mechanistic insight into partitioning dynamics—contrasting equilibrium-seeking compounds against kinetically hindered species—represents a significant advance in understanding the atmospheric behavior of cooking emissions. Our results provide a scientific foundation for refining emission inventories and air quality models, ultimately contributing to improved exposure assessment and mitigation strategies for urban and indoor environments.

Acknowledgement:

This research was supported by the National Key R&D Program of China (2022YFC3701000, Task 2), National Natural Science Foundation of China-Creative Research Group Fund (2222100)

Supplementary Material

Supplementary material is available in the online version of this article.

Author contribution

SG, MH design the research, RS, HW, YY, WZ, ZC, RT, SC perform the experiment, SG, ZW, SL, YC, MH supervise the research, SG provide the research funding, RS, HW, YY analysis the data, RS, SG write the original draft the the manuscript, all the authors review and edit the final manuscript.

Competing interests

Authors declare no competing interests

References

Abdullahi, K. L., Delgado-Saborit, J. M., and Harrison, R. M.: Emissions and indoor concentrations of particulate matter and its specific chemical components from cooking: A review, Atmospheric Environment, 71, 260-294, 10.1016/j.atmosenv.2013.01.061, 2013.

https://doi.org/10.5194/egusphere-2025-6416
Preprint. Discussion started: 31 December 2025
© Author(s) 2025. CC BY 4.0 License.

463 Atkinson, R., Baulch, D. L., Cox, R. A., Crowley, J. N., Hampson, R. F., Hynes, R. G., Jenkin,
464 M. E., Rossi, M. J., Troe, J., and Subcommittee, I.: Evaluated kinetic and photochemical
465 data for atmospheric chemistry: Volume II – gas phase reactions of organic species,
466 Atmos. Chem. Phys., 6, 3625-4055, 10.5194/acp-6-3625-2006, 2006.
467 Bandowe, B. A. M., Lui, K. H., Jones, T., BeruBe, K., Adams, R., Niu, X., Wei, C., Cao, J. J.,
468 Lee, S. C., Chuang, H. C., and Ho, K. F.: The chemical composition and toxicological
469 effects of fine particulate matter (PM(2.5)) emitted from different cooking styles, Environ
470 Pollut, 288, 117754, 10.1016/j.envpol.2021.117754, 2021.
471 Bannan, T. J., Le Breton, M., Priestley, M., Worrall, S. D., Bacak, A., Marsden, N. A., Mehra,
472 A., Hammes, J., Hallquist, M., Alfarra, M. R., Krieger, U. K., Reid, J. P., Jayne, J.,
473 Robinson, W., McFiggans, G., Coe, H., Percival, C. J., and Topping, D.: A method for
474 extracting calibrated volatility information from the FIGAERO-HR-ToF-CIMS and its
475 experimental application, Atmospheric Measurement Techniques, 12, 1429-1439,
476 10.5194/amt-12-1429-2019, 2019.
477 Brown, W. L., Day, D. A., Stark, H., Pagonis, D., Krechmer, J. E., Liu, X., Price, D. J., Katz, E.
478 F., DeCarlo, P. F., Masoud, C. G., Wang, D. S., Hildebrandt Ruiz, L., Arata, C., Lunderberg,
479 D. M., Goldstein, A. H., Farmer, D. K., Vance, M. E., and Jimenez, J. L.: Real-time organic
480 aerosol chemical speciation in the indoor environment using extractive electrospray
481 ionization mass spectrometry, Indoor Air, 31, 141-155, 10.1111/ina.12721, 2021.
482 Buchholz, A., Ylisirniö, A., Huang, W., Mohr, C., Canagaratna, M., Worsnop, D. R.,
483 Schobesberger, S., and Virtanen, A.: Deconvolution of FIGAERO–CIMS thermal desorption
484 profiles using positive matrix factorisation to identify chemical and physical processes
485 during particle evaporation, Atmos. Chem. Phys., 20, 7693-7716, 10.5194/acp-20-7693-
486 2020, 2020.
487 Chandramouli, B., Jang, M., and Kamens, R. M.: Gas–particle partitioning of semi-volatile
488 organics on organic aerosols using a predictive activity coefficient model: analysis of the
489 effects of parameter choices on model performance, Atmospheric Environment, 37, 853-
490 864, 10.1016/s1352-2310(02)00931-7, 2003.
491 Chuang, W. K., and Donahue, N. M.: A two-dimensional volatility basis set – Part 3:
492 Prognostic modeling and NOx dependence, Atmospheric Chemistry and Physics, 16, 123-
493 134, 10.5194/acp-16-123-2016, 2016.

https://doi.org/10.5194/egusphere-2025-6416
Preprint. Discussion started: 31 December 2025
© Author(s) 2025. CC BY 4.0 License.

494 Donahue, N. M., Epstein, S. A., Pandis, S. N., and Robinson, A. L.: A two-dimensional volatility
495 basis set: 1. organic-aerosol mixing thermodynamics, Atmospheric Chemistry and Physics,
496 11, 3303-3318, 10.5194/acp-11-3303-2011, 2011.
497 Donahue, N. M., Kroll, J. H., Pandis, S. N., and Robinson, A. L.: A two-dimensional volatility
498 basis set – Part 2: Diagnostics of organic-aerosol evolution, Atmospheric Chemistry and
499 Physics, 12, 615-634, 10.5194/acp-12-615-2012, 2012.
500 Farmer, D. K., Vance, M. E., Abbatt, J. P. D., Abeleira, A., Alves, M. R., Arata, C., Boedicker,
501 E., Bourne, S., Cardoso-Saldana, F., Corsi, R., DeCarlo, P. F., Goldstein, A. H., Grassian, V.
502 H., Hildebrandt Ruiz, L., Jimenez, J. L., Kahan, T. F., Katz, E. F., Mattila, J. M., Nazaroff,
503 W. W., Novoselac, A., O'Brien, R. E., Or, V. W., Patel, S., Sankhyan, S., Stevens, P. S.,
504 Tian, Y., Wade, M., Wang, C., Zhou, S., and Zhou, Y.: Overview of HOMEChem: House
505 Observations of Microbial and Environmental Chemistry, Environ Sci Process Impacts, 21,
506 1280-1300, 10.1039/c9em00228f, 2019.
507 Guo, S., Hu, M., Peng, J., Wu, Z., Zamora, M. L., Shang, D., Du, Z., Zheng, J., Fang, X., Tang,
508 R., Wu, Y., Zeng, L., Shuai, S., Zhang, W., Wang, Y., Ji, Y., Li, Y., Zhang, A. L., Wang,
509 W., Zhang, F., Zhao, J., Gong, X., Wang, C., Molina, M. J., and Zhang, R.: Remarkable
510 nucleation and growth of ultrafine particles from vehicular exhaust, P Natl Acad Sci USA,
511 117, 3427-3432, 10.1073/pnas.1916366117, 2020.
512 Guo, Z., Chen, X., Wu, D., Huo, Y., Cheng, A., Liu, Y., Li, Q., and Chen, J.: Higher Toxicity of
513 Gaseous Organics Relative to Particulate Matters Emitted from Typical Cooking Processes,
514 Environmental Science & Technology, 57, 17022-17031, 10.1021/acs.est.3c05425, 2023.
515 Hallquist, M., Wenger, J. C., Baltensperger, U., Rudich, Y., Simpson, D., Claeys, M., Dommen,
516 J., Donahue, N. M., George, C., Goldstein, A. H., Hamilton, J. F., Herrmann, H., Hoffmann,
517 T., Iinuma, Y., Jang, M., Jenkin, M. E., Jimenez, J. L., Kiendler-Scharr, A., Maenhaut, W.,
518 McFiggans, G., Mentel, T. F., Monod, A., Prévôt, A. S. H., Seinfeld, J. H., Surratt, J. D.,
519 Szmigielski, R., and Wildt, J.: The formation, properties and impact of secondary organic
520 aerosol: current and emerging issues, Atmos. Chem. Phys., 9, 5155-5236, 10.5194/acp-9-
521 5155-2009, 2009.
522 Hashimoto, S., Takazawa, Y., Ieda, T., Omagari, R., Nakajima, D., Nakamura, S., and Suzuki,
523 N.: Application of rapid air sampling and non-targeted analysis using thermal desorption

https://doi.org/10.5194/egusphere-2025-6416
Preprint. Discussion started: 31 December 2025
© Author(s) 2025. CC BY 4.0 License.

comprehensive two-dimensional gas chromatography/time-of-flight mass spectrometry to accidental fire, Chemosphere, 303, 10.1016/j.chemosphere.2022.135021, 2022.

Iyer, S., Lopez-Hilfiker, F., Lee, B. H., Thornton, J. A., and Kurten, T.: Modeling the Detection of Organic and Inorganic Compounds Using Iodide-Based Chemical Ionization, J Phys Chem A, 120, 576-587, 10.1021/acs.jpca.5b09837, 2016.

Kong, X., Salvador, C. M., Carlsson, S., Pathak, R., Davidsson, K. O., Le Breton, M., Gaita, S. M., Mitra, K., Hallquist, A. M., Hallquist, M., and Pettersson, J. B. C.: Molecular characterization and optical properties of primary emissions from a residential wood burning boiler, Sci Total Environ, 754, 142143, 10.1016/j.scitotenv.2020.142143, 2021.

Le Breton, M., Psichoudaki, M., Hallquist, M., Watne, Å. K., Lutz, A., and Hallquist, Å. M.: Application of a FIGAERO ToF CIMS for on-line characterization of real-world fresh and aged particle emissions from buses, Aerosol Science and Technology, 53, 244-259, 10.1080/02786826.2019.1566592, 2019.

Lee, B. H., Lopez-Hilfiker, F. D., Mohr, C., Kurten, T., Worsnop, D. R., and Thornton, J. A.: An Iodide-Adduct High-Resolution Time-of-Flight Chemical-Ionization Mass Spectrometer: Application to Atmospheric Inorganic and Organic Compounds, Environmental Science & Technology, 48, 6309-6317, 10.1021/es500362a, 2014.

Li, Y., Pöschl, U., and Shiraiwa, M.: Molecular corridors and parameterizations of volatility in the chemical evolution of organic aerosols, Atmospheric Chemistry and Physics, 16, 3327-3344, 10.5194/acp-16-3327-2016, 2016.

Lin, C., Huang, R. J., Duan, J., Zhong, H., and Xu, W.: Polycyclic aromatic hydrocarbons from cooking emissions, Sci Total Environ, 151700, 10.1016/j.scitotenv.2021.151700, 2021.

Liu, W., Zhou, L., Yuan, W., Ruan, L., Wang, X., Guo, Y., Xie, Z., Liu, Q., and Wang, C.: Tracking indoor volatile organic compounds with online mass spectrometry, TrAC Trends Anal. Chem., 171, 10.1016/j.trac.2023.117514, 2024.

Lopez-Hilfiker, F. D., Mohr, C., Ehn, M., Rubach, F., Kleist, E., Wildt, J., Mentel, T. F., Lutz, A., Hallquist, M., Worsnop, D., and Thornton, J. A.: A novel method for online analysis of gas and particle composition: description and evaluation of a Filter Inlet for Gases and AEROsols (FIGAERO), Atmospheric Measurement Techniques, 7, 983-1001, 10.5194/amt-7-983-2014, 2014.

https://doi.org/10.5194/egusphere-2025-6416
Preprint. Discussion started: 31 December 2025
© Author(s) 2025. CC BY 4.0 License.

554 Lopez-Hilfiker, F. D., Mohr, C., D'Ambro, E. L., Lutz, A., Riedel, T. P., Gaston, C. J., Iyer, S.,
555 Zhang, Z., Gold, A., Surratt, J. D., Lee, B. H., Kurten, T., Hu, W. W., Jimenez, J., Hallquist,
556 M., and Thornton, J. A.: Molecular Composition and Volatility of Organic Aerosol in the
557 Southeastern U.S.: Implications for IEPOX Derived SOA, Environ Sci Technol, 50, 2200-
558 2209, 10.1021/acs.est.5b04769, 2016.
559 Lopez-Hilfiker, F. D., Pospisilova, V., Huang, W., Kalberer, M., Mohr, C., Stefenelli, G.,
560 Thornton, J. A., Baltensperger, U., Prevot, A. S. H., and Slowik, J. G.: An extractive
561 electrospray ionization time-of-flight mass spectrometer (EESI-TOF) for online
562 measurement of atmospheric aerosol particles, Atmospheric Measurement Techniques, 12,
563 4867-4886, 10.5194/amt-12-4867-2019, 2019.
564 Lopez-Pedrajas, S., Estevez, R., Schnee, J., Gaigneaux, E. M., Luna, D., and Bautista, F. M.:
565 Study of the gas-phase glycerol oxidehydration on systems based on transition metals (Co,
566 Fe, V) and aluminium phosphate, Molecular Catalysis, 455, 68-77,
567 10.1016/j.mcat.2018.05.020, 2018.
568 Luo, Z., Zang, H., Li, Z., Li, C., and Zhao, Y.: Species-specific effect of particle viscosity and
569 particle-phase reactions on the formation of secondary organic aerosol, Science of The Total
570 Environment, 950, 10.1016/j.scitotenv.2024.175207, 2024.
571 Masoud, C. G., Li, Y., Wang, D. S., Katz, E. F., DeCarlo, P. F., Farmer, D. K., Vance, M. E.,
572 Shiraiwa, M., and Hildebrandt Ruiz, L.: Molecular composition and gas-particle partitioning
573 of indoor cooking aerosol: Insights from a FIGAERO-CIMS and kinetic aerosol modeling,
574 Aerosol Science and Technology, 56, 1156-1173, 10.1080/02786826.2022.2133593, 2022.
575 Mazur, D. M., Detenchuk, E. A., Sosnova, A. A., Artaev, V. B., and Lebedev, A. T.: GC-HRMS
576 with Complementary Ionization Techniques for Target and Non-target Screening for
577 Chemical Exposure: Expanding the Insights of the Air Pollution Markers in Moscow Snow,
578 Science of The Total Environment, 761, 10.1016/j.scitotenv.2020.144506, 2021.
579 Mehra, A., Krechmer, J. E., Lambe, A., Sarkar, C., Williams, L., Khalaj, F., Guenther, A., Jayne,
580 J., Coe, H., and Worsnop, D.: Oligomer and highly oxygenated organic molecule formation
581 from oxidation of oxygenated monoterpenes emitted by California sage plants, Atmospheric
582 Chemistry and Physics, 20, 10953-10965, 10.5194/acp-20-10953-2020, 2020.
583 Milsom, A., Squires, A. M., Boswell, J. A., Terrill, N. J., Ward, A. D., and Pfrang, C.: An
584 organic crystalline state in ageing atmospheric aerosol proxies: spatially resolved structural

https://doi.org/10.5194/egusphere-2025-6416
Preprint. Discussion started: 31 December 2025
© Author(s) 2025. CC BY 4.0 License.

changes in levitated fatty acid particles, Atmospheric Chemistry and Physics, 21, 15003-15021, 10.5194/acp-21-15003-2021, 2021.

Nolte, C. G., Schauer, J. J., Cass, G. R., and Simoneit, B. R. T.: Highly Polar Organic Compounds Present in Meat Smoke, Environmental Science & Technology, 33, 3313-3316, 10.1021/es990122v, 1999.

Peng, Z., Day, D. A., Ortega, A. M., Palm, B. B., Hu, W., Stark, H., Li, R., Tsigaridis, K., Brune, W. H., and Jimenez, J. L.: Non-OH chemistry in oxidation flow reactors for the study of atmospheric chemistry systematically examined by modeling, Atmos. Chem. Phys., 16, 4283-4305, 10.5194/acp-16-4283-2016, 2016.

Peng, Z., and Jimenez, J. L.: Radical chemistry in oxidation flow reactors for atmospheric chemistry research, Chem Soc Rev, 49, 2570-2616, 10.1039/c9cs00766k, 2020.

Pozza, S. A., Gonçalves, P. B., Wouters, F. C., Vendemiatti, J. A. S., Nogarotto, D. C., Pereira-Filho, E. R., Osório, D. M. M., Romualdo, L. L., Godoi, J. R., Hoinaski, L., and Urban, R. C.: Particulate matter pollution and non-targeted analysis of polar compounds in three regions of Brazil, Chemosphere, 341, 10.1016/j.chemosphere.2023.139839, 2023.

Reyes-Villegas, E., Bannan, T., Le Breton, M., Mehra, A., Priestley, M., Percival, C., Coe, H., and Allan, J. D.: Online Chemical Characterization of Food-Cooking Organic Aerosols: Implications for Source Apportionment, Environ Sci Technol, 52, 5308-5318, 10.1021/acs.est.7b06278, 2018.

Rogge, W. F., Hildemann, L. M., Mazurek, M. A., Cass, G. R., and Simoneit, B. R. T.: Sources of fine organic aerosol. 1. Charbroilers and meat cooking operations, Environmental Science & Technology, 25, 1112-1125, 10.1021/es00018a015, 1991.

Röhler, L., Schlabach, M., Haglund, P., Breivik, K., Kallenborn, R., and Bohlin-Nizzetto, P.: Non-target and suspect characterisation of organic contaminants in Arctic air – Part 2: Application of a new tool for identification and prioritisation of chemicals of emerging Arctic concern in air, Atmospheric Chemistry and Physics, 20, 9031-9049, 10.5194/acp-20-9031-2020, 2020.

Schervish, M., and Shiraiwa, M.: Impact of phase state and non-ideal mixing on equilibration timescales of secondary organic aerosol partitioning, Atmospheric Chemistry and Physics, 23, 221-233, 10.5194/acp-23-221-2023, 2023.

https://doi.org/10.5194/egusphere-2025-6416
Preprint. Discussion started: 31 December 2025
© Author(s) 2025. CC BY 4.0 License.

615 Schymanski, E. L., Singer, H. P., Slobodnik, J., Ipolyi, I. M., Oswald, P., Krauss, M., Schulze,
616 T., Haglund, P., Letzel, T., Grosse, S., Thomaidis, N. S., Bletsou, A., Zwiener, C., Ibáñez,
617 M., Portolés, T., de Boer, R., Reid, M. J., Onghena, M., Kunkel, U., Schulz, W., Guillon, A.,
618 Noyon, N., Leroy, G., Bados, P., Bogialli, S., Stipaničev, D., Rostkowski, P., and Hollender,
619 J.: Non-target screening with high-resolution mass spectrometry: critical review using a
620 collaborative trial on water analysis, Analytical and Bioanalytical Chemistry, 407, 6237-
621 6255, 10.1007/s00216-015-8681-7, 2015.
622 Shiraiwa, M., Pfrang, C., Koop, T., and Pöschl, U.: Kinetic multi-layer model of gas-particle
623 interactions in aerosols and clouds (KM-GAP): linking condensation, evaporation and
624 chemical reactions of organics, oxidants and water, Atmospheric Chemistry and Physics, 12,
625 2777-2794, 10.5194/acp-12-2777-2012, 2012.
626 Song, K., Guo, S., Gong, Y., Lv, D., Wan, Z., Zhang, Y., Fu, Z., Hu, K., and Lu, S.: Non-target
627 scanning of organics from cooking emissions using comprehensive two-dimensional gas
628 chromatography-mass spectrometer (GC×GC-MS), Appl. Geochem., 151,
629 10.1016/j.apgeochem.2023.105601, 2023a.
630 Song, K., Tang, R., Li, A., Wan, Z., Zhang, Y., Gong, Y., Lv, D., Lu, S., Tan, Y., Yan, S., Yan,
631 S., Zhang, J., Fan, B., Chan, C. K., and Guo, S.: Particulate organic emissions from incense-
632 burning smoke: Chemical compositions and emission characteristics, Science of The Total
633 Environment, 897, 10.1016/j.scitotenv.2023.165319, 2023b.
634 Takhar, M., Li, Y., and Chan, A. W. H.: Characterization of secondary organic aerosol from
635 heated-cooking-oil emissions: evolution in composition and volatility, Atmospheric
636 Chemistry and Physics, 21, 5137-5149, 10.5194/acp-21-5137-2021, 2021.
637 Takhar, M., Li, Y., Ditto, J. C., and Chan, A. W. H.: Formation pathways of aldehydes from
638 heated cooking oils, Environ Sci Process Impacts, 10.1039/d1em00532d, 2022.
639 Tikkanen, I. P., Buchholz, A., Ylisirniö, A., Schobesberger, S., Virtanen, A., and Yli-Juuti, T.:
640 Comparing secondary organic aerosol (SOA) volatility distributions derived from isothermal
641 SOA particle evaporation data and FIGAERO-CIMS measurements, Atmospheric
642 Chemistry and Physics, 20, 10441-10458, 10.5194/acp-20-10441-2020, 2020.
643 Wang, H., Guo, S., Yu, Y., Shen, R., Zhu, W., Tang, R., Tan, R., Liu, K., Song, K., Zhang, W.,
644 Zhang, Z., Shuai, S., Xu, H., Zheng, J., Chen, S., Li, S., Zeng, L., and Wu, Z.: Secondary
645 aerosol formation from a Chinese gasoline vehicle: Impacts of fuel (E10, gasoline) and

https://doi.org/10.5194/egusphere-2025-6416
Preprint. Discussion started: 31 December 2025
© Author(s) 2025. CC BY 4.0 License.

646 driving conditions (idling, cruising), Sci Total Environ, 795,
647 10.1016/j.scitotenv.2021.148809, 2021.
648 Yang, Y., Yang, L., Zheng, M., Cao, D., and Liu, G.: Data acquisition methods for non-targeted
649 screening in environmental analysis, TrAC Trends in Analytical Chemistry, 160,
650 10.1016/j.trac.2023.116966, 2023.
651 Ylisirniö, A., Barreira, L. M. F., Pullinen, I., Buchholz, A., Jayne, J., Krechmer, J. E., Worsnop,
652 D. R., Virtanen, A., and Schobesberger, S.: On the calibration of FIGAERO-ToF-CIMS:
653 importance and impact of calibrant delivery for the particle-phase calibration, Atmospheric
654 Measurement Techniques, 14, 355-367, 10.5194/amt-14-355-2021, 2021.
655 Yu, Y., Guo, S., Wang, H., Shen, R. Z., Zhu, W. F., Tan, R., Song, K., Zhang, Z. R., Li, S. D.,
656 Chen, Y. F., and Hu, M.: Importance of Semivolatile/Intermediate-Volatility Organic
657 Compounds to Secondary Organic Aerosol Formation from Chinese Domestic Cooking
658 Emissions, Environ Sci Tech Let, 9, 507-512, 10.1021/acs.estlett.2c00207, 2022.
659 Zaveri, R. A., Shilling, J. E., Zelenyuk, A., Liu, J., Bell, D. M., D'Ambro, E. L., Gaston, C. J.,
660 Thornton, J. A., Laskin, A., Lin, P., Wilson, J., Easter, R. C., Wang, J., Bertram, A. K.,
661 Martin, S. T., Seinfeld, J. H., and Worsnop, D. R.: Growth Kinetics and Size Distribution
662 Dynamics of Viscous Secondary Organic Aerosol, Environmental Science & Technology,
663 52, 1191-1199, 10.1021/acs.est.7b04623, 2018.
664 Zeng, J., Yu, Z., Mekic, M., Liu, J., Li, S., Loisel, G., Gao, W., Gandolfo, A., Zhou, Z., Wang,
665 X., Herrmann, H., Gligorovski, S., and Li, X.: Evolution of Indoor Cooking Emissions
666 Captured by Using Secondary Electrospray Ionization High-Resolution Mass Spectrometry,
667 Environmental Science & Technology Letters, 7, 76-81, 10.1021/acs.estlett.0c00044, 2020.
668 Zhang, H., Yee, L. D., Lee, B. H., Curtis, M. P., Worton, D. R., Isaacman-VanWertz, G.,
669 Offenberg, J. H., Lewandowski, M., Kleindienst, T. E., Beaver, M. R., Holder, A. L.,
670 Lonneman, W. A., Docherty, K. S., Jaoui, M., Pye, H. O. T., Hu, W., Day, D. A.,
671 Campuzano-Jost, P., Jimenez, J. L., Guo, H., Weber, R. J., de Gouw, J., Koss, A. R.,
672 Edgerton, E. S., Brune, W., Mohr, C., Lopez-Hilfiker, F. D., Lutz, A., Kreisberg, N. M.,
673 Spielman, S. R., Hering, S. V., Wilson, K. R., Thornton, J. A., and Goldstein, A. H.:
674 Monoterpenes are the largest source of summertime organic aerosol in the southeastern
675 United States, Proc Natl Acad Sci U S A, 115, 2038-2043, 10.1073/pnas.1717513115, 2018.

https://doi.org/10.5194/egusphere-2025-6416
Preprint. Discussion started: 31 December 2025
© Author(s) 2025. CC BY 4.0 License.

676 Zhang, X., Pandis, S. N., and Seinfeld, J. H.: Diffusion-Limited Versus Quasi-Equilibrium
677 Aerosol Growth, Aerosol Science and Technology, 46, 874-885,
678 10.1080/02786826.2012.679344, 2012.
679 Zhu, W., Guo, S., Zhang, Z., Wang, H., Yu, Y., Chen, Z., Shen, R., Tan, R., Song, K., Liu, K.,
680 Tang, R., Liu, Y., Lou, S., Li, Y., Zhang, W., Zhang, Z., Shuai, S., Xu, H., Li, S., Chen, Y.,
681 Hu, M., Canonaco, F., and Prévôt, A. S. H.: Mass spectral characterization of secondary
682 organic aerosol from urban cooking and vehicular sources, Atmos. Chem. Phys., 21, 15065-
683 15079, 10.5194/acp-21-15065-2021, 2021.

684